



**HAL**  
open science

## Impact of soil moisture on the long-term energy performance of an earth-air heat exchanger system

Jian Lin, Hossein Nowamooz, Sandrine Braymand, Patrice Wolff, Christophe Fond

### ► To cite this version:

Jian Lin, Hossein Nowamooz, Sandrine Braymand, Patrice Wolff, Christophe Fond. Impact of soil moisture on the long-term energy performance of an earth-air heat exchanger system. *Renewable Energy*, 2018, 10.1016/j.renene.2018.06.106 . hal-02387639

**HAL Id: hal-02387639**

**<https://hal.science/hal-02387639>**

Submitted on 21 Jul 2022

**HAL** is a multi-disciplinary open access archive for the deposit and dissemination of scientific research documents, whether they are published or not. The documents may come from teaching and research institutions in France or abroad, or from public or private research centers.

L'archive ouverte pluridisciplinaire **HAL**, est destinée au dépôt et à la diffusion de documents scientifiques de niveau recherche, publiés ou non, émanant des établissements d'enseignement et de recherche français ou étrangers, des laboratoires publics ou privés.



Distributed under a Creative Commons Attribution - NonCommercial 4.0 International License

# 1 Impact of soil moisture on the long-term energy performance of an 2 earth-air heat exchanger system

3 Jian Lin<sup>a</sup>, Hossein Nowamooz<sup>b</sup>, Sandrine Braymand<sup>a</sup>, Patrice Wolff<sup>a</sup>, Christophe Fond<sup>a</sup>

4 <sup>a</sup> ICUBE, UMR 7357, CNRS, IUT Robert Schuman, University of Strasbourg, 72 Route du Rhin, 67400  
5 Illkirch-Graffenstaden, France

6 <sup>b</sup> ICUBE, UMR 7357, CNRS, INSA Strasbourg, 24 Boulevard de la Victoire, 67084 Strasbourg, France

---

## 7 Abstract

The soil moisture contents affect significantly the soil thermal properties and consequently the thermal efficiency of shallow geothermal systems. This effect becomes more complex to be evaluated for an Earth-Air Heat Exchanger (EAHE) because of its non-stable energy performance due to a large fluctuation of the temperature of air. In this study, the impact of soil moisture content and soil thermal properties has been investigated on the long-term energy performance of an instrumented EAHE site. First, a full-scale experimental EAHE site in University of Strasbourg as well as its measured data are presented. The thermal properties of different soil layers present in the site were experimentally and theoretically characterized with different soil moisture contents. Based on these results, an analytical solution was proposed to simulate the soil temperature of the field and the output air temperature of the EAHE. A computer program based on this analytical solution was developed to assess the performance of the system for a period of three years. The numerical calculation was validated for an average saturation condition by comparing simulation results with measured data. Different soil saturation conditions were also used in the numerical simulation to consider the effect of soil moisture on the system performance. The results show that if the turbulent flow of the circulating air is fully developed, the difference of the exchanged energy could reach more than 40%.

8 *Keywords:* Shallow geothermal system, Earth-air heat exchanger, Full-scale experimental  
9 site, Long-term energy performance, Soil moisture

---

## 10 Nomenclature

11	$\alpha$	soil thermal diffusivity	$[m^2.s^{-1}]$
12	$\chi$	soil texture dependent parameter for $K_C$	
13	$\gamma_d$	soil dry density	$[kN.m^{-3}]$
14	$\kappa$	soil texture dependent parameter for $K_\lambda$	
15	$\lambda_{air}$	air thermal conductivity	$[W.m^{-1}.K^{-1}]$
16	$\lambda_{soil}$	soil thermal conductivity	$[W.m^{-1}.K^{-1}]$

17	$\mu_{air}$	air dynamic viscosity	$[kg.m^{-1}.s^{-1}]$
18	$\omega$	pulsation frequency	$[s^{-1}]$
19	$\phi$	heat exchange power	$[W]$
20	$\rho_{air}$	air density	$[kg.m^{-3}]$
21	$\varphi$	phase shift of a pulsation	$[rad]$
22	$A$	amplitude of a temperature pulsation	$[^{\circ}C]$
23	$C_{soil}$	soil volumetric heat capacity	$[J.m^{-3}.K^{-1}]$
24	$Cp_{air}$	air specific heat capacity	$[J.m^{-3}.K^{-1}]$
25	$E$	cumulated heat exchange energy	$[kWh]$
26	$e$	soil thickness	$[m]$
27	$K_C$	normalized heat capacity	
28	$K_{\lambda}$	normalized thermal conductivity	
29	$L_{pipe}$	length of the pipe	$[m]$
30	$P$	electric power of the guarded-hot-plate device	$[W]$
31	$Q$	heat exchange	$[J]$
32	$q$	thermal flux	$[W]$
33	$q'$	thermal flux per unit length for the pipe	$[W.m^{-1}]$
34	$R$	cylindrical thermal resistance	$[m.K.W^{-1}]$
35	$r_{pipe}$	radius of pipe	$[m]$
36	$r_{pipe}$	radius of the pipe	$[m]$
37	$S$	surface of soil samples in guarded-hot-plate device	$[m^2]$
38	$Sr$	degree of saturation of soils	$[\%]$
39	$T$	temperature of a medium	$[^{\circ}C]$
40	$t$	time	$[s]$
41	$x$	horizontal distance from pipe inlet	$[m]$
42	$x_s$	sand content of soils	$[\%]$
43	$z$	depth from ground surface	$[m]$

## 44 1. Introduction

45 Geothermal energy, using the ground as a heat source, is a renewable energy that can  
46 be used to provide heating and cooling for buildings. As one of the shallow geothermal so-  
47 lutions, earth-air heat exchanger(EAHE) system is considered as an energy efficient method  
48 for preheating and cooling of the air supplied to a building [1][2][3].

49 An EAHE geothermal system is usually composed of one or some pipes buried horizontally  
50 to a depth from  $1m$  to  $3m$  and either around or under the building. As the position of heat  
51 exchangers is close to the ground surface, the water content of the soil layer can be strongly  
52 impacted by the climatic solicitations such as rainwater precipitation or evapo-transpiration.  
53 These solicitations modify the hydraulic conditions of the soil profile and the underground  
54 water level [4][5][6].

55 Furthermore, it is well known that soil thermal properties depend on soil type and porosity,  
56 solid particle conductivity, gas pressure and especially soil moisture content. Woodside and  
57 Messmer have studied the thermal conductivity of unconsolidated sands in [7]. They showed  
58 that the effective thermal conductivity varies with porosity, solid particle conductivity, sat-  
59 urating fluid conductivity, and the pressure of the saturating gas. Tavman [8] have taken  
60 into account the grain size in the thermal conductivity model for construction sands. Abu-  
61 Hamdeh [9] have investigated the effect of water content and bulk density on the specific  
62 heat, volumetric heat capacity, and thermal diffusivity of some sieved and repacked soils  
63 through laboratory studies. Usowicz et al. [10] presented regression equations for predicting  
64 thermal conductivity based on easily measured quantities such as penetration resistance and  
65 water content or air-filled porosity. Lipiec et al. [11] have assessed the effects of tilled and  
66 grass covered soil on the spatial distribution of the thermal properties. The results showed  
67 that in general the spatial distributions of both thermal conductivity and heat capacity were  
68 similar to those of water content. Davarzani et al. [12] have studied experimentally and  
69 theoretically the effect of solid thermal conductivity and particle-particle contact on ther-  
70 modiffusion processes of a saturated porous medium. They showed that compared with the  
71 particle-particle contact, the porosity had more impact on the thermodiffusion coefficients.  
72 Gori and Corasaniti [13] have proposed a model to evaluate the effective thermal conduc-  
73 tivity of three-phase soils. The proposed model, which depended on porosity and degree of  
74 saturation, could predict the effective thermal conductivity with a good agreement. Niki-  
75 forova et al. [14] have studied the thermophysical characteristics of different soil types. They  
76 showed that the thermal conductivity depended on different types (sand, clay and loam) and  
77 humidity of soil. Nowamooz et al. [15] have investigated the heat distribution throughout  
78 the profile of unsaturated multilayered soil. Water content, dry density and sand content of  
79 the soil profile were used to estimate soil thermal properties.

80 The influence of these soil hydro-thermal variations around the horizontal geothermal heat  
81 exchanger system have been studied by several works. These studies have been carried out to  
82 assess the energy performance of the entire geothermal heat exchanger system with time and  
83 space. Leong et al.[16] studied the effect of soil type and moisture content on a ground heat  
84 pump performance. The performance of a ground heat pump system was found to depend  
85 strongly on moisture content and soil type. Mohamed et al. [17] investigated experimen-  
86 tally the effects of circulating coolant flow rate, groundwater table fluctuations, infiltration  
87 of rainwater, on the amount of thermal energy that can be recovered from the near surface

88 soil layers. They showed that the infiltration of rainwater causes a temporary enhancement  
89 on the amount of extracted heat. Gao et al. [18] studied thermal performance improvement  
90 of a horizontal ground-coupled heat exchanger by rainwater harvest. A horizontal ground-  
91 coupled heat exchanger was combined with a rain garden which increased soil moisture. The  
92 benefit of the supply of rainwater was confirmed by experimental results. The performance  
93 of ground coupled heat exchangers in unsaturated soils has been studied by Platts et al.  
94 [19]. Their work showed that the soil thermal properties such as thermal conductivity and  
95 diffusivity influenced significantly the efficiency of the heat exchanger system. Di Sipio and  
96 Bertermann [20] have carried out a field test of horizontal helical heat exchangers. Change  
97 of soil moisture content in the same climatic conditions and under the same thermal stress  
98 for five different soil mixtures have been monitored in the test site.

99 However, most of these studies focused on the ground-coupled heat exchanger (GCHE) with  
100 earth-liquid exchanger, whilst few have studied the impact of soil moisture content on thermal  
101 efficiency of EAHE systems. Vaz et al.[21] have constructed and monitored an experimental  
102 EAHE system to study the use of soil as a energy reservoir. Gan [22][23][24] proposed a  
103 numerical model of EAHE which takes into account interactions between the heat exchanger  
104 and the soil and atmosphere. By performing a simulation over one month during winter in  
105 [23], he showed that when the interactions between the heat exchanger, soil and ventilating  
106 air were neglected the thermal performance of the EAHE would be over predicted. Recently,  
107 Cuny et al. [25] have carried out a study on the influence of coating soil types on the energy  
108 of an EAHE. They compared the exchanged energies of an EAHE in January and July with  
109 three different soil types surrounding the exchanger pipe. The results showed that a mix of  
110 sand and bentonite could reduce significantly the fluctuation of soil moisture content and  
111 guarantee a stable energy performance. In fact, the assessment of the energy performance of  
112 an EAHE system is more complex compared to the assessment of an GCHE system. Indeed,  
113 heat exchange medium is the air extracted directly from the external environment which  
114 represents a great range of temperature fluctuation.

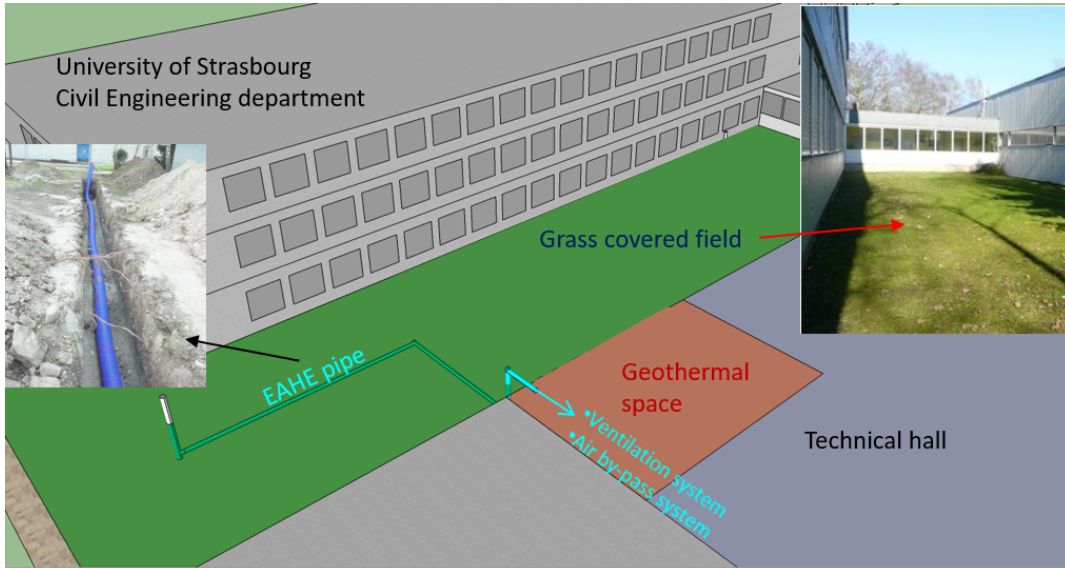
115 Furthermore, there is no research work in the literature which investigates the energy perfor-  
116 mance of the EAHE system for more than one year. Based on three years' recorded data of  
117 an instrumented full-scale EAHE site, this study considers the impact of moisture conditions  
118 of different soil layers on the long-term energy performance of an EAHE system. First, the  
119 site used for the installation of the EAHE system is described. The thermal properties' char-  
120 acterisation for the site's different soil layers, by using experimental methods and a proposed  
121 theoretical estimation, is presented. To assess the energy performance of the EAHE system,  
122 a numerical model was built by considering the system hydro-thermal behaviour. The model  
123 was validated by comparing the simulation results and the measured data. To analyze the  
124 effect of soil moisture content, the estimated soil thermal properties at dry and saturated  
125 conditions were used in the numerical model to estimate the evolution of the exchanged en-  
126 ergy of the entire EAHE system.

127

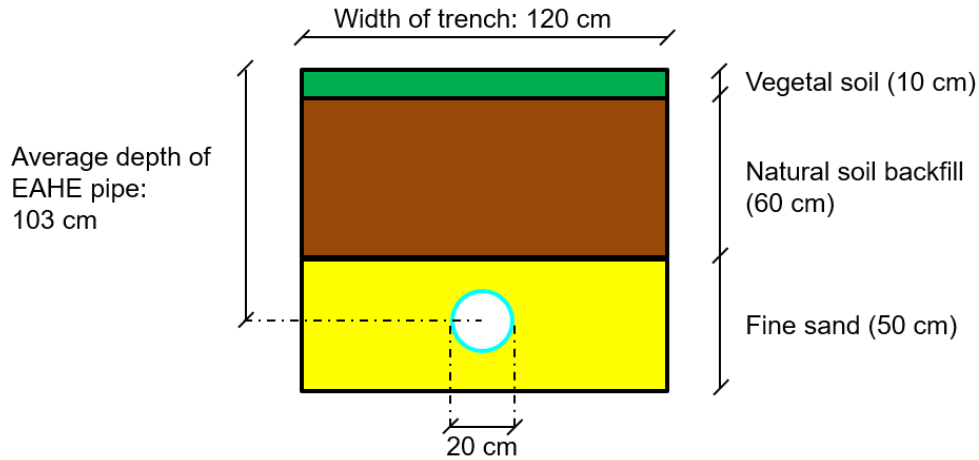
128 **2. Description of the EAHE system and experimental field measurements**

129 An experimental EAHE system was constructed in 2012 at the University of Strasbourg  
 130 in France<sup>1</sup>. As shown in Figure 1, an air-earth exchanger pipe was buried in a field between  
 131 two civil engineering department buildings. The soil profile is composed of 3 layers: 10 cm  
 132 of vegetal soil, 60 cm of natural soil backfill, and about 50 cm of fine sand around the pipe.  
 133 The average buried depth of exchanger pipe is 1.03 m.

During the operation of the EAHE system, external air is extracted and fed into the EAHE



a) Global view of the site



b) Soil profile of trench

Figure 1: Experimental EAHE site

<sup>1</sup>Funded by the European Commission Initiative INTERREG IV, Upper Rhine Programme (Project B20-TEM3)

134 which is composed of a polyethylene pipe. The outer diameter of the pipe is 20 *cm* and  
 135 its inner diameter is 17 *cm*. The total length of the EAHE pipe is 17.5 *m*. To avoid the  
 136 overconsumption of ventilation energy, a by-pass system is associated to the EAHE to allow  
 137 the outside air to bypass the EAHE pipe when the external air temperature is close to soil  
 138 temperature. For this study, a low blowing velocity(0.51 *m/s*) was applied to obtain greater  
 139 thermal exchange time between air and earth. The input and output air temperatures were  
 140 measured with PT100 temperature sensors and recorded every 20 minutes by a Keithley  
 141 3706A data logger. Figure 2 shows the evolution of the input and output air temperature of  
 142 the EAHE system recorded from July 2012 to August 2017.

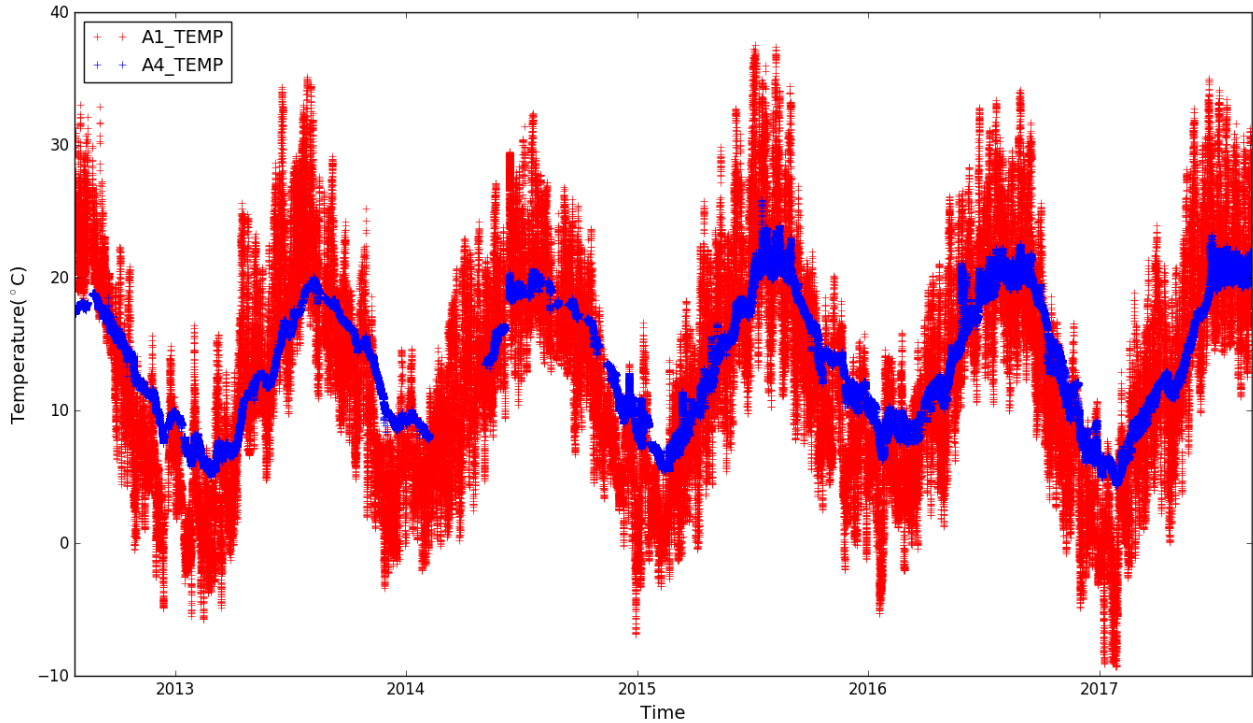


Figure 2: Input and output air temperature of the EAHE system from July 2012 to August 2017 (Input air temperature: Sensor A1-TEMP; Output air temperature: Sensor A4-TEMP)

143

### 144 3. Research methodology

#### 145 3.1. Experimental characterization of soil thermal properties

146 According to different soil textures, two experimental methods were used to characterize  
 147 the soil thermal properties. A heat-pulse dual-probe(HPDP) sensor was used for the vegetal  
 148 soil as well as the fine sand with the grain size smaller than 5 *mm*. For natural soil backfill,  
 149 a guarded-hot-plate method was preferred.

- 150 a) Test method for fine texture soils (vegetal soil and fine sand) : “KD2 pro” HPDP sensor
- 151 The soil was put into a column with an inner diameter of 50 *mm* and a height of
- 152 100 *mm* to a desired bulk density. Soil samples were sealed and placed in a room held

153  
154  
155  
156  
157  
158  
159  
160  
161  
162

at a constant temperature ( $20 \pm 1 \text{ }^\circ\text{C}$ ) for 24 hours before the taking of measurements to ensure the thermal equilibrium between water and soil. A hand-held device named KD2 Pro was used to measure the thermal properties of the packed soil columns. A dual needle SH-1 sensor with a length of  $30 \text{ mm}$  and a diameter of  $1.3 \text{ mm}$  was used to measure the thermal conductivity  $\lambda_{soil}$  and the volumetric heat capacity of the soils  $C_{soil}$  [26]. It was carefully inserted into each soil column, and electric current was applied to the sensor which produced a heat pulse (see Figure 3). Heat-pulse measurements were repeated two times on each soil column. Soil thermal properties ( $\lambda_{soil}$  and  $C_{soil}$ ) were determined with an algorithm for the dual needle probe based on the line heat source analysis given in [27, 28]. After the measurements were taken, soil columns were oven dried at  $105 \text{ }^\circ\text{C}$  for 24 hours to determine water moisture content.

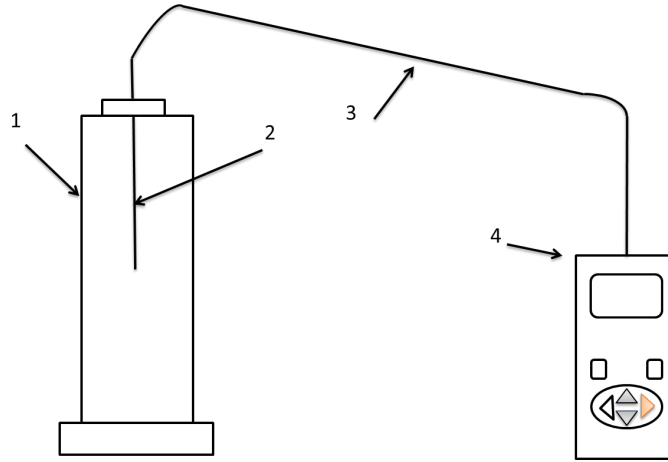


Figure 3: Scheme of KD2 Pro thermal properties analyser: (1) mould, (2) SH-1 sensor, (3) cable, (4) micro-controller.

163  
164  
165  
166  
167  
168  
169

- b) Test method for coarse texture soils (natural soil backfill) : guarded-hot-plate device  
As shown in Figure 4, a guarded-hot-plate test [29] was used for the soil for which the size of the greatest soil particle is superior to the distance between the dual needles of the “KD2 Pro” device ( $5 \text{ mm}$ ). Plate size is  $40 \text{ cm} \times 60 \text{ cm}$ . The thickness of insulations under the hot plate and around the sample is about  $10 \text{ cm}$  to ensure an unidimensional thermal transfer.

170  
171  
172  
173  
174

Soil samples with a thickness between  $5 \text{ cm}$  and  $7 \text{ cm}$  were installed between hot and cold plates. At thermal equilibrium, a constant heat flow was applied to soil samples at a stationary temperature state. Soil thermal conductivity  $\lambda_{soil}$  was then determined by heat flow, the mean temperature difference between the samples’ surfaces and their dimensions:

$$\lambda_{soil} = \frac{P \times e}{S \times (T_1 - T_2)} \quad (1)$$

175  
176  
177  
178

where  $P$  is the measured electric power of the hot plate,  $e$  and  $S$  are the thickness and the surface of soil samples,  $T_1$  and  $T_2$  represent respectively the temperatures of the hot and cold plates.

The same test apparatus was used to measure the soil volumetric heat capacity  $C_{soil}$

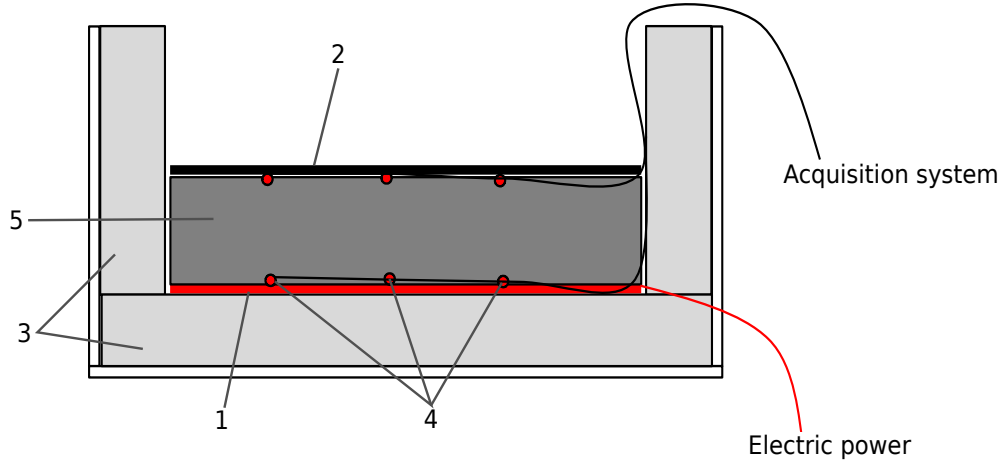


Figure 4: Scheme of hot plate test apparatus: (1) hot plate, (2) cold plate, (3) insulations, (4) temperature sensors, (5) soil sample

179 with the help of an insulation cover of 10 *cm* on the soil samples:

$$C_{soil} = \frac{P \times t}{V \times (T_f - T_i)} \quad (2)$$

180 where  $P$  is the power of the hot plate,  $t$  is the duration of tests,  $V$  is the volume of soil  
 181 samples,  $T_i$  and  $T_f$  represent respectively the initial and final mean temperature of soil  
 182 samples.

183

### 184 3.2. Theoretical approach for soil thermal properties

185 For each soil layer, the thermal properties were measured at 3 different saturation states.  
 186 However, to estimate the soil thermal properties at other degrees of saturation, it was nec-  
 187 essary to know their evolutions with soil moisture content. In this part, a theoretical rela-  
 188 tionship for the soil thermal conductivity  $\lambda_{soil}$  and capacity  $C_{soil}$  compared with degree of  
 189 saturation is proposed. The concept of normalized thermal conductivity  $K_\lambda$  proposed by [30]  
 190 was used:

$$\lambda_{soil} = (\lambda_{soil}^{sat} - \lambda_{soil}^{dry})K_\lambda + \lambda_{soil}^{dry} \quad (3)$$

191 where  $\lambda_{soil}^{dry}$  and  $\lambda_{soil}^{sat}$  are the thermal conductivity of dry and saturated soils.

192 The measured thermal conductivity values for the 3 soil layers of the EAHE site were used  
 193 to calibrate the proposed model. A set of linear relationships of  $\lambda_{soil}^{sat}$  and  $\lambda_{soil}^{dry}$  was proposed  
 194 for fitting functions adapted to that data:

$$\begin{aligned} \lambda_{soil}^{sat} &= a_1 x_s + b_1 \gamma_d \\ \lambda_{soil}^{dry} &= c_1 x_s + d_1 \gamma_d \end{aligned} \quad (4)$$

195 where  $x_s$  and  $\gamma_d$  are sand content and dry density of soils,  $a_1$  and  $b_1$  fitted parameters for sat-  
 196 urated thermal conductivity are respectively  $0.53W.m^{-1}.K^{-1}$  and  $0.1W.m^2.K^{-1}.(kN)^{-1}$ , and  
 197 where  $c_1$  and  $d_1$  fitted parameters for dry thermal conductivity are respectively  $0.087W.m^{-1}.K^{-1}$   
 198 and  $0.019W.m^2.K^{-1}.(kN)^{-1}$ .

199 To relate normalized thermal conductivity  $K_\lambda$  to the degree of saturation  $S_r$ , the equation  
 200 proposed by Coté and Konrad [31] was used:

$$K_\lambda = \frac{\kappa S_r}{1 + (\kappa - 1)S_r} \quad (5)$$

201 Here,  $\kappa$  is a texture dependent parameter which varies linearly with sand content  $x_s$ :

$$\kappa = e_1 x_s + f_1 \quad (6)$$

202 where  $e_1$  and  $f_1$  are parameters fitted with the measured data. They are respectively 4.4 and  
 203 0.4.

204 To propose a theoretical model for the soil heat capacity  $C_{soil}$ , the normalized heat capacity  
 205  $K_C$  concept was used:

$$C_{soil} = (C_{soil}^{sat} - C_{soil}^{dry})K_C + C_{soil}^{dry} \quad (7)$$

206 where  $C_{soil}^{dry}$  and  $C_{soil}^{sat}$  are the heat capacity of dry and saturated soils.

207 Using the measured data and following the same procedure as that for  $K_\lambda$ , a set of linear  
 208 relationships for the fitting functions were proposed:

$$\begin{aligned} C_{soil}^{sat} &= a_2 \gamma_d - b_2 x_s \\ C_{soil}^{dry} &= c_2 \gamma_d - d_2 x_s \end{aligned} \quad (8)$$

209 where  $a_2$  and  $b_2$  fitted parameters for saturated heat capacity are respectively  $7.5 \times 10^4$   
 210  $J.(kN)^{-1}.K^{-1}$  and  $1 \times 10^4 J.m^{-3}.K^{-1}$ , and where  $c_2$  and  $d_2$  fitted parameters for dry heat  
 211 capacity are respectively  $1.9 \times 10^5 J.(kN)^{-1}.K^{-1}$  and  $1 \times 10^5 J.m^{-3}.K^{-1}$ .

212 To relate normalized heat capacity  $K_C$  to the degree of saturation  $S_r$ , a linear equation was  
 213 used:

$$K_C = S_r \chi \quad (9)$$

214 Here,  $\chi$  is a texture dependent parameter which varied linearly with sand content  $x_s$ :

$$\chi = e_2 x_s + f_2 \quad (10)$$

215 where  $e_2$  and  $f_2$  are fitted parameters. They are respectively 0.05 and 1.0.

### 216 3.3. Numerical simulation of the EAHE system

217 In this section, taking into consideration the soil thermal properties of each layer, the  
 218 numerical simulation of the experimental EAHE system is presented. In the numerical cal-  
 219 culations, the soil temperature around the exchanger pipe was first estimated by using the  
 220 surface air temperature and the soil thermal properties. The output air temperature was  
 221 calculated by considering a transient thermal transfer between soil, exchanger pipe and air  
 222 inside the exchanger.

223 *3.3.1. Surrounding soil temperature at the buried depth of the exchanger pipe*

224 Homogeneous soil condition was first considered. According to a semi-infinite condition,  
 225 the soil temperature at the buried depth of the heat exchanger pipes was estimated by the  
 226 following transient, heat conduction equation:

$$227 \frac{\partial^2 T_{soil}(z, t)}{\partial z^2} = \frac{1}{\alpha} \times \frac{\partial T_{soil}(z, t)}{\partial t} \quad (11)$$

228 where  $\alpha$  is the soil thermal diffusivity which is calculated by  $\alpha = \lambda_{soil}/C_{soil}$ , and  $z$  is the depth  
 229 below ground surface. The corresponding boundary condition at  $z = 0$  is the ambient air  
 230 temperature at the soil surface. According to a recent study on the analytical expression of  
 231 ambient air at our experimental site [32], a function composed of annual and daily pulsations  
 232 of temperature, taking into account of annual variation of daily amplitude, was proposed:

$$233 T_{soil}(0, t) = T_{air}^{amb}(t) \quad (12)$$

$$= T_m + A_0 \cdot \sin(\omega_y t + \varphi_0) + (A_m + A_1 \cdot \sin(\omega_y t + \varphi_1)) \cdot \sin(\omega_d t + \varphi_2)$$

234 where  $T_m$  and  $A_m$  are the annual averages of temperature and daily amplitude,  $A_0$  and  
 235  $A_1$  represent respectively the annual amplitude of air temperature wave and daily varia-  
 236 tion amplitude,  $\omega_y = 2\pi/(365 \cdot 24 \cdot 3600) \text{ s}^{-1}$  is the annual pulsation frequency and  $\omega_d =$   
 237  $2\pi/(24 \cdot 3600) \text{ s}^{-1}$  is the daily pulsation frequency,  $\varphi_0$ ,  $\varphi_1$  and  $\varphi_2$  are phase shifts of these  
 238 three pulsations.

239 By using the expression (12), the solution of the equation (11) is obtained:

$$240 T_{soil}(z, t) = T_m + A_0 e^{-\sqrt{\frac{\omega_y}{2\alpha}} \cdot z} \cdot \sin\left(\omega_y t + \varphi_0 - \sqrt{\frac{\omega_y}{2\alpha}} \cdot z\right)$$

$$+ A_m e^{-\sqrt{\frac{\omega_d}{2\alpha}} \cdot z} \cdot \sin\left(\omega_d t + \varphi_2 - \sqrt{\frac{\omega_d}{2\alpha}} \cdot z\right) \quad (13)$$

$$+ A_1 e^{-\sqrt{\frac{\omega_y + \omega_d}{2\alpha}} \cdot z} \cdot \left[ \sin\left(\omega_d t + \varphi_2 - \sqrt{\frac{\omega_y + \omega_d}{2\alpha}} \cdot z\right) \cdot \sin(\omega_y t + \varphi_1) \right]$$

241 as daily frequency  $\omega_d$  is much greater than the annual frequency  $\omega_y$  ( $\omega_d = 365 \times \omega_y$ ),  $\omega_y + \omega_d \approx$   
 242  $\omega_d$ , then the expression of soil temperature is simplified by:

$$243 T_{soil}(z, t) = T_m + A_0 e^{-\sqrt{\frac{\omega_y}{2\alpha}} \cdot z} \cdot \sin\left(\omega_y t + \varphi_0 - \sqrt{\frac{\omega_y}{2\alpha}} \cdot z\right) \quad (14)$$

$$+ (A_m + A_1 \cdot \sin(\omega_y t + \varphi_1)) e^{-\sqrt{\frac{\omega_d}{2\alpha}} \cdot z} \cdot \sin\left(\omega_d t + \varphi_2 - \sqrt{\frac{\omega_d}{2\alpha}} \cdot z\right)$$

244 As soil in the experimental EAHE site is multilayered (Figure 1), the expression of soil  
 245 temperature at the buried depth of exchanger pipe is extended from the equation (14):

$$\begin{aligned}
T_{soil}(z, t) = & T_m + A_0 e^{-\sqrt{\frac{\omega_y}{2\alpha_1}} z_1 - \sqrt{\frac{\omega_y}{2\alpha_2}} z_2 - \sqrt{\frac{\omega_y}{2\alpha_3}} (z - z_1 - z_2)} \cdot \\
& \sin\left(\omega_y t + \varphi_0 - \sqrt{\frac{\omega_y}{2\alpha_1}} z_1 - \sqrt{\frac{\omega_y}{2\alpha_2}} z_2 - \sqrt{\frac{\omega_y}{2\alpha_3}} (z - z_1 - z_2)\right) + \\
& (A_m + A_1 \sin(\omega_y t + \varphi_1)) e^{-\sqrt{\frac{\omega_d}{2\alpha_1}} z_1 - \sqrt{\frac{\omega_d}{2\alpha_2}} z_2 - \sqrt{\frac{\omega_d}{2\alpha_3}} (z - z_1 - z_2)} \cdot \\
& \sin\left(\omega_d t + \varphi_2 - \sqrt{\frac{\omega_d}{2\alpha_1}} z_1 - \sqrt{\frac{\omega_d}{2\alpha_2}} z_2 - \sqrt{\frac{\omega_d}{2\alpha_3}} (z - z_1 - z_2)\right)
\end{aligned} \tag{15}$$

247 where  $z$  represents the buried depth of the pipe;  $z_1$  and  $z_2$  are the layer thickness of the  
248 vegetal soil and the natural soil backfill;  $\alpha_1$ ,  $\alpha_2$  and  $\alpha_3$  represent respectively the thermal  
249 diffusivity of vegetal soil, natural soil backfill and fine sand.

### 250 3.3.2. Simulation of the heat transfer from soil to air

251 Once the soil temperature at the depth of earth-air exchanger was determined, the air  
252 temperature inside the pipe and its evolution along the length of the exchanger was calculated  
253 by using the three hypotheses described below.

254 First, it was considered that the thermal exchange is in a quasi-stationary state for each  
255 simulation instant  $t$ , which represents 20 minutes i.e. equal to the length of time between  
256 two data records. Second, there is a zone surrounding the pipe where the soil temperature  
257 is disturbed by the thermal exchange and so the soil temperature outside this zone is only  
258 impacted and determined by the surface temperature, as shown in the equation (15). Third,  
259 the air flow inside the exchanger pipe remains turbulent. Therefore, the thermal exchange  
260 between the pipe's wall and the air is considered as a forced convection.

261 Figure 5 shows the thermal exchange schema of a segment  $dx$  of the EAHE exchanger, where  
262  $\overline{T_{soil}}(t)$  is the soil temperature at the average buried depth of the exchanger pipe,  $T_{air}(x, t)$   
263 and  $T_{air}(x + dx, t)$  represent respectively the air temperature before and after this segment of  
264 pipe,  $r_{pipe}^{ext}$  and  $r_{pipe}^{int}$  are the external and the inner radius of the pipe,  $v_{air}$  signifies air velocity.

265 In the radial direction, thermal flux per length unit  $q'$  is expressed as:

$$q' = q/dx = \frac{\overline{T_{soil}}(t) - T_{air}(x, t)}{R_{cond} + R_{conv}} \tag{16}$$

266 where  $R_{cond}$  is the thermal conduction resistance from the soil to the inner side of pipe, and  
267  $R_{conv}$  represents the thermal convection resistance between the inner wall of pipe and the  
268 flowing air.  $R_{cond}$  is composed of the thermal resistance of impacted surrounding soil and the  
269 pipe. Its expression is:

$$R_{cond} = R_{soil} + R_{pipe} = \frac{\ln[(r_{pipe}^{ext} + e_{soil})/r_{pipe}^{ext}]}{2\pi\lambda_{soil}} + \frac{\ln(r_{pipe}^{ext}/r_{pipe}^{int})}{2\pi\lambda_{pipe}} \tag{17}$$

271 where  $r_{pipe}^{ext}$  and  $r_{pipe}^{int}$  represent respectively the inner and outer radius of pipe, and as proposed  
272 by [33],  $e_{soil}$  is the thickness of soil layer impacted by the heat exchanger:

$$e_{soil} = \sqrt{2\alpha/\omega_d} \tag{18}$$

273 where  $\alpha$  is the soil thermal diffusivity within this thermal penetration thickness, and  $\omega_d$  is  
274 the daily pulsation frequency.

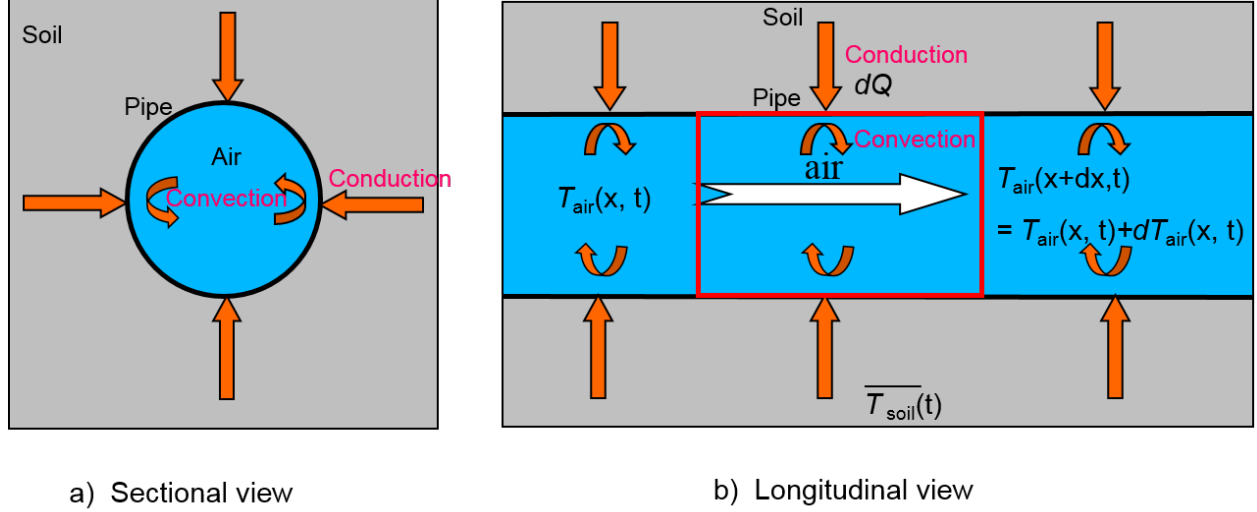


Figure 5: Thermal exchange schema of a segment of the EAHE pipe

275 The thermal convection resistance inside the pipe  $R_{conv}$  is expressed as:

276

$$R_{conv} = R_{air} = \frac{1}{2\pi r_{pipe}^{int} \cdot h_{air}} \quad (19)$$

277 Here the convective heat transfer coefficient  $h_{air}$  depends on dimensionless numbers  $Re$ ,  
278  $Pr$  and  $Nu$ . According to [34] [35], their relations are:

279

$$\begin{aligned} Re &= \frac{v_{air} \rho_{air} 2r_{pipe}^{int}}{\mu_{air}} \\ Pr &= \frac{\mu_{air} C_{p_{air}}}{\lambda_{air}} \\ Nu &= \frac{(f/8) Re Pr}{1 + 12.7 \sqrt{f/8} (Pr^{2/3} - 1)} \quad \text{with: } f = (0.78 \ln Re - 1.5)^{-2} \\ h_{air} &= \frac{Nu \lambda_{air}}{2r_{pipe}^{int}} \end{aligned} \quad (20)$$

280 where  $\rho_{air}$  is the air density,  $\mu_{air}$  is the air dynamic viscosity,  $\lambda_{air}$  and  $C_{p_{air}}$  represent re-  
281 spectively the thermal conductivity and the specific heat capacity of air.

282 In the direction of the flowing air, the heat exchange  $dQ$  between the surrounding soil to the  
283 air for this segment of pipe  $dx$  is written by:

284

$$dQ = q \frac{dx}{v_{air}} = q' \frac{d^2x}{v_{air}} = \frac{\overline{T_{soil}(t)} - T_{air}(x, t)}{R_{soil} + R_{pipe} + R_{air}} \quad (21)$$

285 Therefore the change of air temperature between the input and output of this pipe segment  
286  $dx$  is obtained:

287

$$\begin{aligned}
dT_{air}(x, t) &= T_{air}(x + dx, t) - T_{air}(x, t) \\
&= \frac{dQ}{C_p^{air} \rho_{air} \pi r_{pipe}^{int\ 2} dx} \\
&= \frac{\overline{T_{soil}}(t) - T_{air}(x, t)}{(R_{soil} + R_{pipe} + R_{air}) v_{air} C_p^{air} \rho_{air} \pi r_{pipe}^{int\ 2}} dx
\end{aligned} \tag{22}$$

288

By resolving the equation (22) an analytical solution is obtained:

289

$$\begin{aligned}
T_{air}(x, t) &= \overline{T_{soil}}(t) + [T_{air}(0, t) - \overline{T_{soil}}(t)] e^{-\tilde{A}x} \\
\text{with: } \tilde{A} &= \left[ (R_{soil} + R_{pipe} + R_{air}) v_{air} C_p^{air} \rho_{air} \pi r_{pipe}^{int\ 2} \right]^{-1}
\end{aligned} \tag{23}$$

290

It is assumed that the input air temperature is equal to the ambient air temperature:

291

$$T_{air}(0, t) = T_{air}^{in}(t) = T_{air}^{amb}(t) \tag{24}$$

292

Therefore, the output air temperature of the EAHE for the required instant  $t$  is expressed by:

293

$$T_{air}^{out}(t) = T_{air}(L_{pipe}, t) = \overline{T_{soil}}(t) + [T_{air}^{amb}(t) - \overline{T_{soil}}(t)] e^{-\tilde{A}L_{pipe}} \tag{25}$$

294

where  $L_{pipe}$  is the length of the exchanger pipe.

295

### 3.3.3. Numerical program

296

A computer program, written in language PYTHON, has been developed to simulate the EAHE system.

297

298

To obtain the analytical function of the soil temperature at the depth of the EAHE pipe (15), an analytical function (12) was required to represent ambient air temperature. The parameters of this function were obtained with the help of the recorded outside air temperature data. A curve fitting following the least square method was developed in the program.

299

300

301

The output air temperature of the EAHE system was calculated for each recorded instant by using the proposed analytical model presented in section 3.3.2. The series of equations (from equation (16) to equation (25)) was programmed to simulate the output air temperature for the whole period. The by-pass process of the whole EAHE ventilation system was taken into account to perform the simulations. When the by-pass system, associated to the EAHE, is activated, the air is extracted directly from outside. In this case, the output air temperature is equal to the outside ambient air temperature.

302

303

304

305

306

307

308

309

310

## 4. Results and discussion

311

### 4.1. Thermal properties of different soil layers of the EAHE site

312

313

314

315

316

The experimental results of the soil thermal properties were then simulated by the aforementioned theoretical approaches (see Figures 6 and 7) using the sand content and dry density of each layer presented in Table 1. The comparison between the approaches and the experimental results demonstrates a good performance of the proposed approaches to estimate soil thermal conductivity and heat capacity.

317

Table 1: Particle-size distribution and dry density for 3 soil types

Soil type	Sand content $x_s(\%)$	Dry density $\gamma_d(kN.m^{-3})$
Vegetal soil	35	13.5
Fine sand	50	14.2
Natural soil	80	16

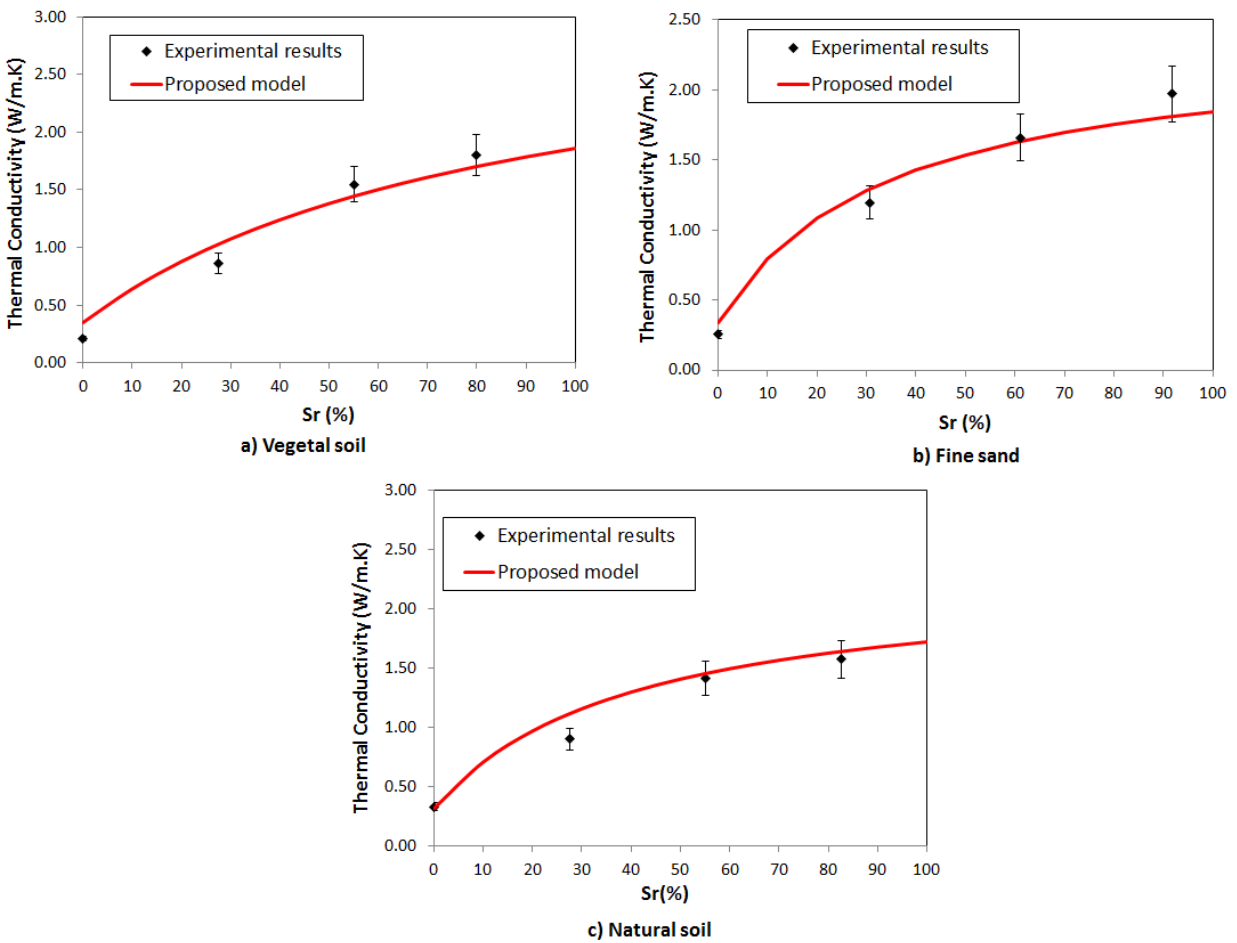


Figure 6: Theoretical predictions and experimental measurements of the soil thermal conductivity: a) vegetal soil, b) fine sand, c) natural soil backfill

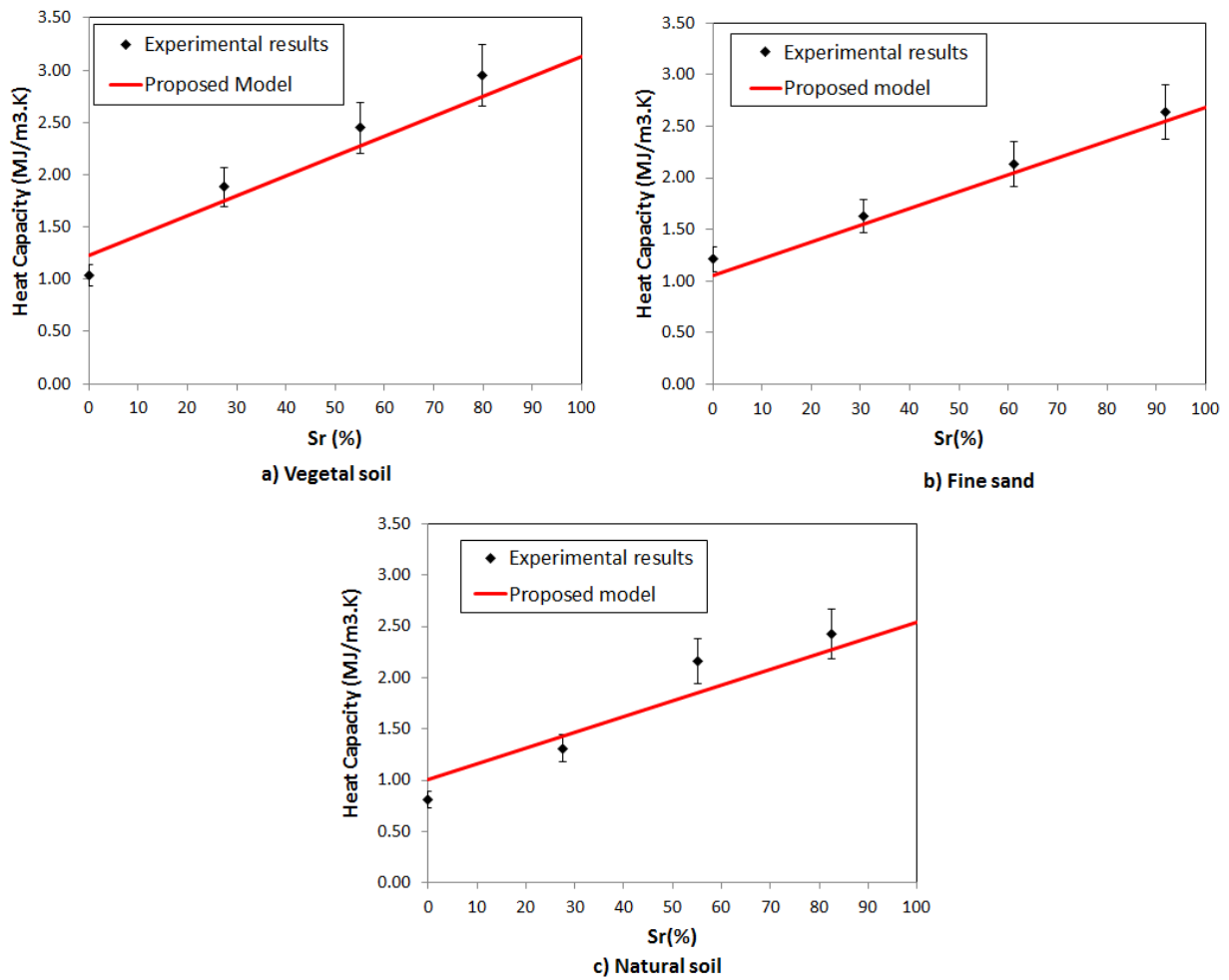


Figure 7: Theoretical predictions and experimental measurements of the soil heat capacity: a) vegetal soil, b) fine sand, c) natural soil backfill

318 *4.2. Simulation results of the EAHE system*

319 In this part, the simulation results are presented for soil temperature, output air temper-  
 320 ature and the cumulated exchanged of the EAHE energy. The simulation period was 3 years:  
 321 from July 13th 2014 to July 13th 2017. For this period the recorded data exists for all the  
 322 sensors.

323 *4.2.1. Soil temperature*

324 To estimate the soil temperature at the depth of the EAHE pipe, an analytical function  
 325 (12) was required to represent ambient air temperature. The parameters of this function  
 326 were obtained by a curve fitting of the recorded outside air temperature data from July 13th  
 327 2014 to July 13th 2017. Besides the annual pulsation frequency  $\omega_y = 2\pi/(365 \cdot 24 \cdot 3600) s^{-1}$   
 328 and the daily pulsation frequency  $\omega_d = 2\pi/(24 \cdot 3600) s^{-1}$ , other necessary parameters are  
 329 shown in table 2. Figure 8 shows the comparison between the simulation function and the  
 330 measured results of the ambient air temperature. Some rupture zones are observed on the  
 331 curves. These rupture zones are due to a lack of data for these periods because of different  
 332 technical problems.

Table 2: Obtained parameters for the external ambient air temperature expression

$T_m$ [ $^{\circ}C$ ]	$A_0$ [ $^{\circ}C$ ]	$A_m$ [ $^{\circ}C$ ]	$A_1$ [ $^{\circ}C$ ]	$\varphi_0$ [rad]	$\varphi_1$ [rad]	$\varphi_2$ [rad]
13.40	-9.43	-3.52	2.10	4.63	-1.25	1.00

334 The soil thermal properties corresponding to the average degree of saturation were used in  
 335 the simulations. Their values were estimated by using the proposed approach in section 3.2.  
 336 With the ambient air temperature expression(equation (12)) and the soil thermal properties  
 337 presented in Table 3, the equation (15) was used to calculate soil temperature at the average  
 338 buried depth of the EAHE pipe with  $z = 1.03 m$ . Figure 9 shows the comparison between  
 339 the estimated soil temperature and measured values at the same depth. It can be seen that  
 simulation results are in accordance with recorded data.

Table 3: Estimated soil thermal properties at average degree of saturation

<b>Soil type</b>	<b>Average degree of saturation</b> $Sr[\%]$	<b>Thermal conductivity</b> $\lambda_{soil}[W.m^{-1}.K^{-1}]$	<b>Thermal capacity</b> $C_{soil}[MJ.m^{-3}.K^{-1}]$	<b>Thermal diffusivity</b> $\alpha_{soil} = \lambda_{soil}/C_{soil}$ $[m^2.s^{-1}]$
Vegetal soil	57.8	1.48	2.33	$0.64 \times 10^{-6}$
Fine sand	18	1.50	1.80	$0.83 \times 10^{-6}$
Natural soil	33.0	1.20	1.51	$0.79 \times 10^{-6}$

340

341 *4.2.2. Output air temperature of the EAHE system*

342  $T_{air}^{out}$  was calculated from each measured input air temperature  $T_{air}^{in}$  that had been previ-  
 343 ously recorded every 20 minutes. Figure 10 shows the comparison between the simulation

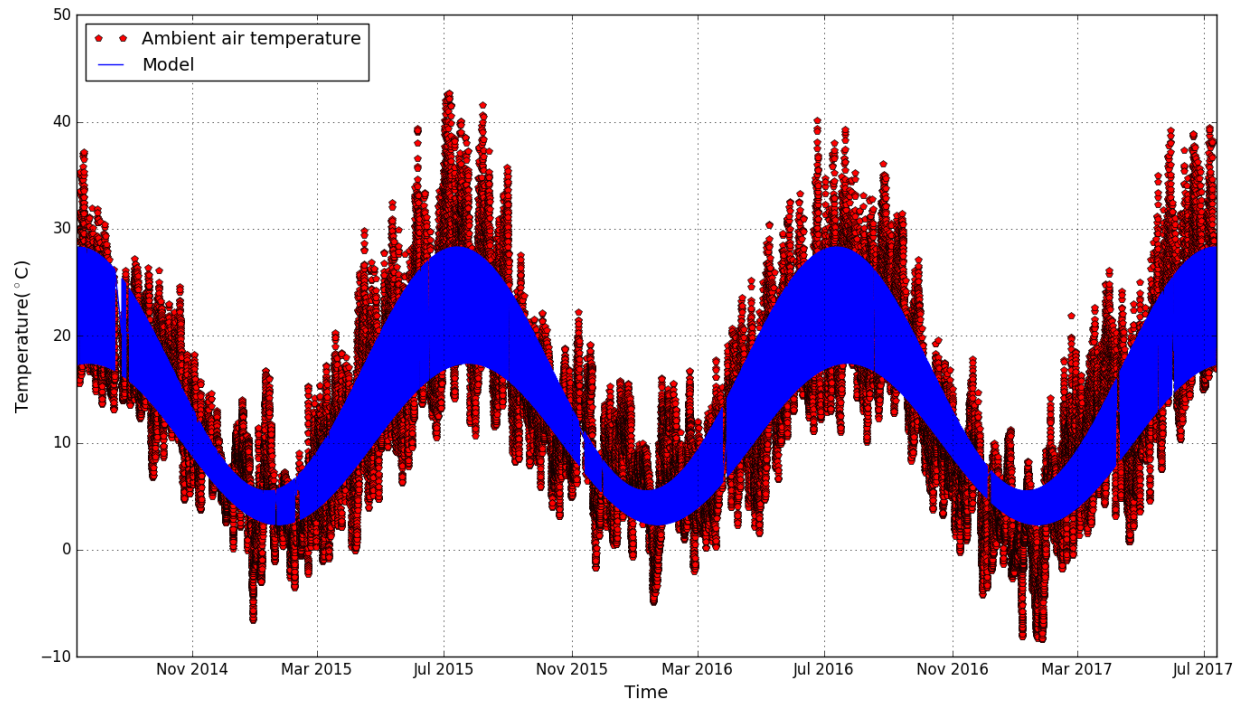


Figure 8: Curve fitting of the external air temperature

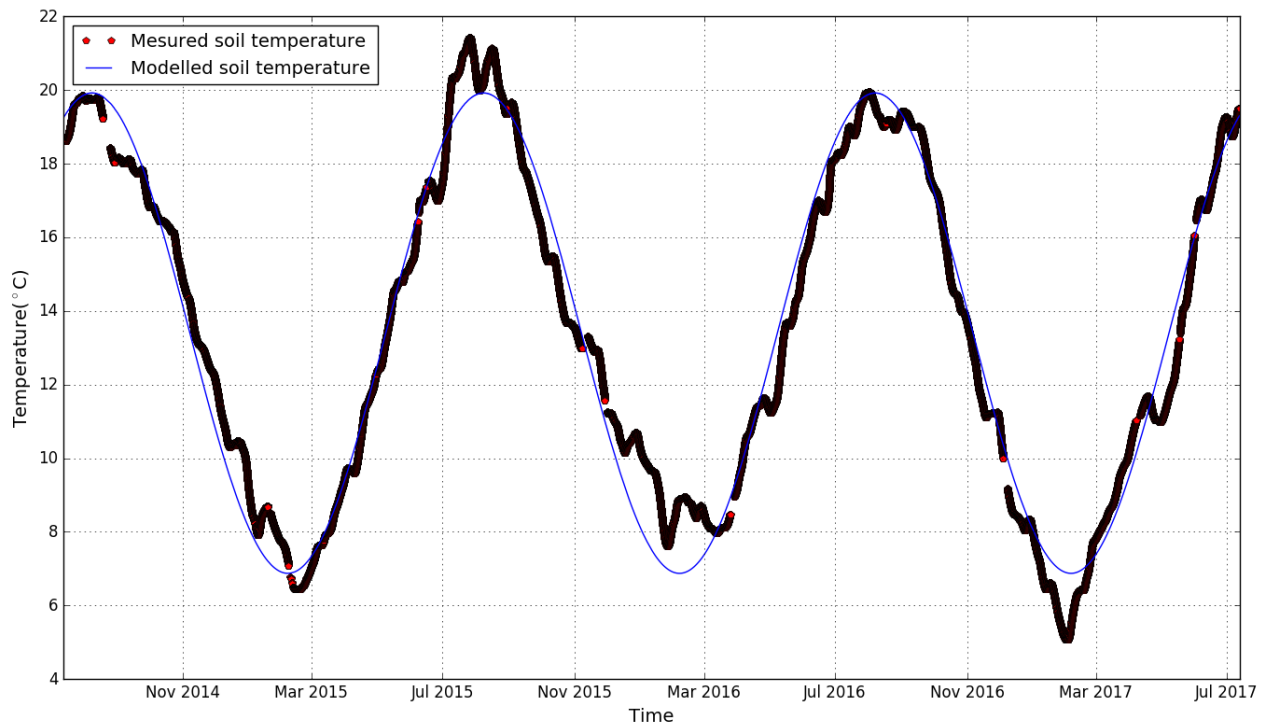


Figure 9: Modeling of the external air temperature

344 results and the recorded data with zooms for winter (from November 2015 to February 2016)  
 345 and summer (from June to September 2016) periods. For the whole period, a standard devi-  
 346 ation of  $0.69\text{ }^{\circ}\text{C}$  was obtained. This shows an appropriate prediction of the proposed model.  
 347 Nevertheless, compared with summer periods, a more remarkable difference is noticed for  
 348 winter periods. It may be due to the non-consideration of the thermal flux coming from the  
 349 underfloor of the nearby building which was heated during winter.

350

#### 351 4.2.3. Cumulated exchanged energy of the EAHE system

352 To assess the global energy performance of the EAHE system, the heat exchange energy  
 353 for 3 years was calculated by using the following equation:

$$E = \int \phi(t)dt \quad (26)$$

354 where  $\phi(t)$  is the power of the heat exchange at each instant  $t$ . It was obtained by:

$$\phi(t) = v_{air}\pi (r_{pipe}^{int})^2 C_{p_{air}} [T_{air}^{in}(t) - T_{air}^{out}(t)] \quad (27)$$

355 To distinguish the heating mode in winter and the cooling mode in summer, the heating  
 356 energy was computed when the output air temperature  $T_{air}^{out}$  was higher than the input air  
 357 temperature  $T_{air}^{in}$  while the cooling energy was added when  $T_{air}^{out}$  was less than  $T_{air}^{in}$ .

Table 4 shows the exchanged energy derived from measured and modelled data. A good

Table 4: Cumulated exchanged energy for three years derived from measured and modelled data at average moisture conditions

Exchanged Energy	Values calculated from experimental data [kWh]	Values calculated from simulated data [kWh]	Relative difference [%]
Cooling Energy	244	242	0.82
Heating Energy	477	433	9.22

358

359 performance of the proposed model is confirmed with the differences under 10 % between  
 360 the calculated and measured exchanged energy. For the cumulated cooling energy, produced  
 361 essentially in summer, this difference is even less than 1 %. As for the simulated output air  
 362 temperature in winter, a greater difference is noticed for the cumulated heating energy. The  
 363 neglecting of the heat transfer of the nearby heated underfloor during winter is probably the  
 364 reason for this even greater difference.

365

#### 366 4.3. Discussion of soil moisture content effects

367 Two extreme conditions, dry and saturated, of the surrounding soil were tested in the  
 368 numerical simulations to assess the effect of soil moisture content on the long-term energy  
 369 performance of the EAHE system. The evolution of thermal conductivity and capacity for  
 370 the multi-layered soils was considered by the analytical approach proposed in section 3.2.

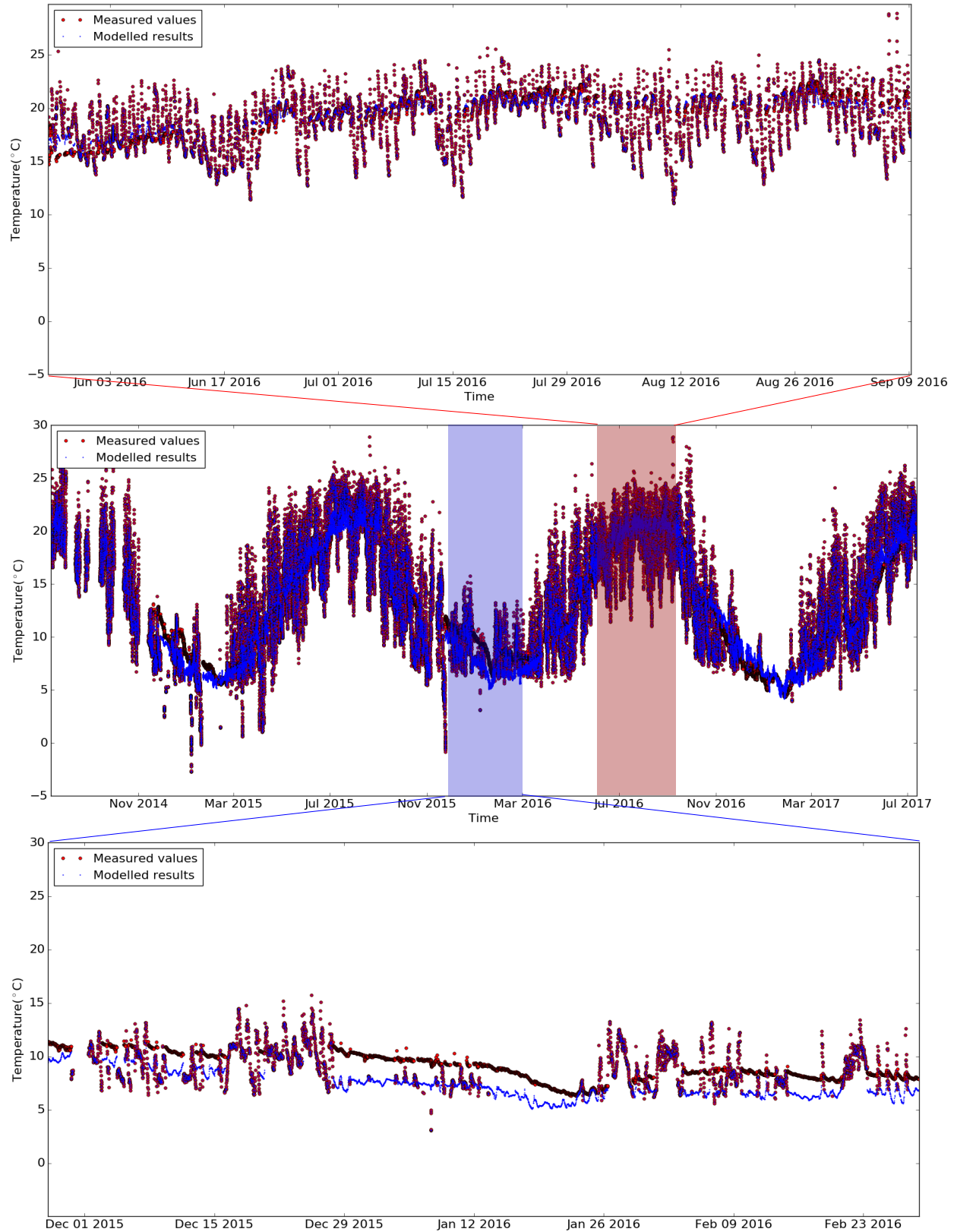


Figure 10: Comparison between the modelled results and the measured values for the EAHE output air temperature

371 Their values as well as the derived thermal diffusivity at dry and saturated conditions are  
 372 shown in Table 5.

Table 5: Thermal properties of different soil layers at dry and water saturation conditions

Soil type	Degree of saturation $Sr[\%]$	Thermal conductivity $\lambda_{soil}[W.m^{-1}.K^{-1}]$	Thermal capacity $C_{soil}[MJ.m^{-3}.K^{-1}]$	Thermal diffusivity $\alpha_{soil} = \lambda_{soil}/C_{soil}$ $[m^2.s^{-1}]$
Vegetal soil	0	0.35	1.23	$0.28 \times 10^{-6}$
Vegetal soil	100	1.86	3.13	$0.59 \times 10^{-6}$
Sand	0	0.34	1.06	$0.32 \times 10^{-6}$
Sand	100	1.84	2.68	$0.69 \times 10^{-6}$
Natural soil	0	0.32	1.01	$0.32 \times 10^{-6}$
Natural soil	100	1.72	2.55	$0.67 \times 10^{-6}$

373  
 374 The heating and cooling exchanged energies of the EAHE in dry and saturated conditions  
 375 were calculated for the period from July 13th 2014 to July 13th 2017, by using the same air  
 376 velocity and ambient air temperature. The results are shown in Table 6.

Table 6: Cumulated exchanged energy for three years derived from modelled data at dry and saturation conditions

	Exchanged En- ergy at dry condition [kWh]	Exchanged En- ergy at saturation condition [kWh]	Relative difference [%]
Colling Energy	256	252	1.56
Heating Energy	472	453	4.03

377  
 378 When air velocity is  $0.51 m/s$ , it is shown in Table 6 that the exchanged energies at the  
 379 dry condition are a little higher than those at the saturated condition. This phenomenon can  
 380 be explained by the soil thermal diffusivity values shown in Table 5. The thermal diffusivity  
 381 values of three soil layers at the dry condition are lower than their values at the saturated  
 382 condition. Since the soil temperature at the buried depth of the exchanger pipe, calculated by  
 383 equation (15), depends directly on the soil thermal diffusivity. A more important difference  
 384 between the input air temperature and the soil temperature is found for soils with a lower  
 385 thermal diffusivity. It means that the thermal exchange potential at the dry condition is  
 386 more than that of the saturated condition. Meanwhile, the obtained output air temperature  
 387 is also influenced by the soil thermal conductivity. The thermal exchange flux  $q$ , calculated  
 388 by equation (16), depends not only on the difference between the input air temperature and  
 389 the soil temperature at the buried depth of pipe but also on the soil thermal resistance  $R_{soil}$ .  
 390 The higher the moisture content in soil layers, the higher the soil thermal conductivity (see  
 391 Table 5) and the less the soil thermal resistance  $R_{soil}$ . When the air velocity is  $0.51 m/s$ , the

392 change of thermal exchange potential due to soil moisture variation dominats the variation  
 393 of thermal flux  $q$ , thus the calculated exchanged energy.

394 Moreover, the impact of soil moisture is very little in this case. A difference of less than  
 395 5% between the dry and saturated conditions is observed. This is due to the insignificant  
 396 variation of soil thermal resistance  $R_{soil}$  with the change of soil moisture compared to the  
 397 combined thermal resistance ( $R_{soil} + R_{pipe} + R_{air}$ ). Since the pipe thermal resistance  $R_{pipe}$   
 398 is constant and small, the entire thermal resistance is mainly related to the air convection  
 399 resistance  $R_{air}$  inside the pipe. In fact, the estimated air convection resistance  $R_{air}$  for the  
 400 experimental site is high due to the low air velocity value ( $v_{air} = 0.51 \text{ m/s}$ ). This low velocity  
 401 was set to ensure an upper exchanging time between the air and earth and therefore an out-  
 402 put air temperature closer to the soil temperature. In the simulations, the Reynolds number  
 403 corresponding to this air velocity is equal to 5740 representing a turbulent flow ( $Re > 4000$ ).  
 404 However, the fully developed turbulent flow ( $Re > 10000$ ) that is necessary for an optimized  
 405 thermal exchange was not reached [34].

406 For this reason, the energy performance of EAHE was also computed by using different air ve-  
 407 locities varying from  $1.0 \text{ m/s}$  (with  $Re = 11255$ ) to  $4.0 \text{ m/s}$  (with  $Re = 45020$ ), which is the  
 408 maximum recommended value to avoid a too great pressure loss and over energy consumption  
 409 of ventilation reported in the German Guideline - Direct thermal use of underground [36].

Figures 11 and 12 show respectively the cumulated cooling and heating exchanged energy

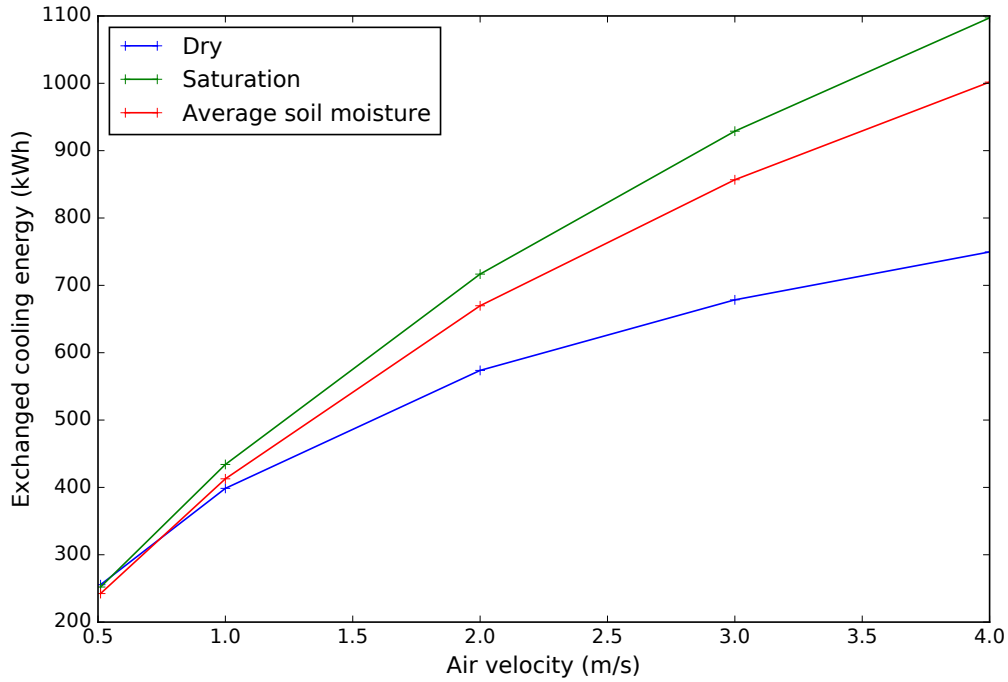


Figure 11: Graph of the cumulated EAHE cooling energy (from 2014-07-13 to 2017-07-13) with different air velocities at different saturation conditions

410 of the EAHE system at different air velocities (from  $0.51 \text{ m/s}$  to  $4.0 \text{ m/s}$ ) for three years.  
 411 The exchanged energies for the soil with an average moisture content (see Table 4) are also  
 412 presented in these figures. At a low air circulation velocity of  $0.51 \text{ m/s}$ , the three soil mois-  
 413

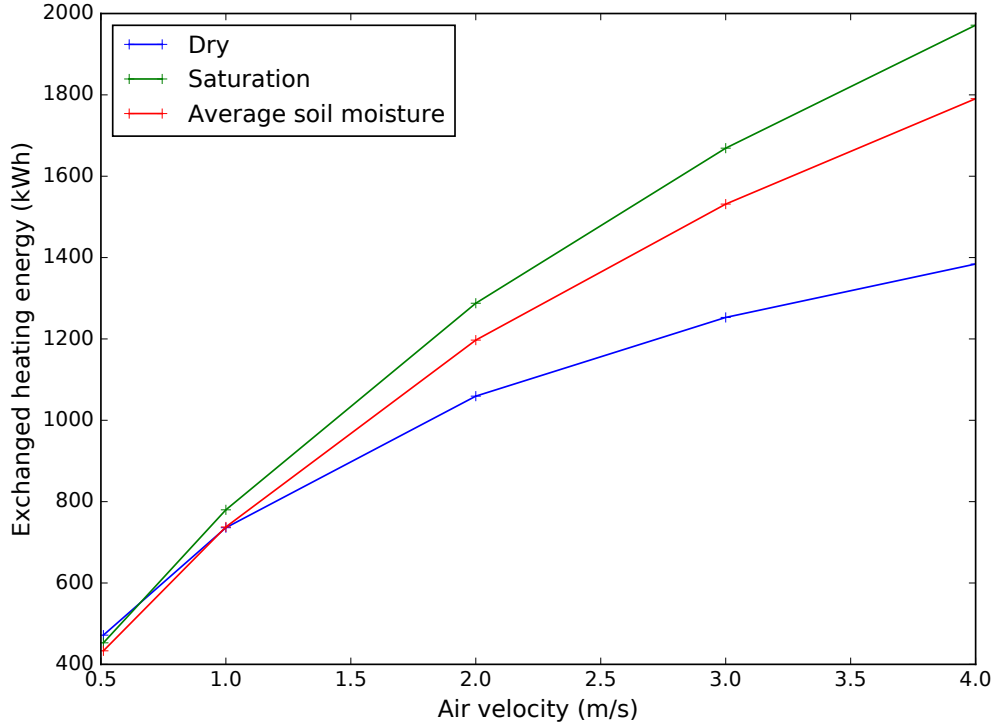


Figure 12: Graph of the cumulated EAHE heating energy (from 2014-07-13 to 2017-07-13) with different air velocities at different saturation conditions

414 ture conditions present almost the same cumulated exchanged energy, and the impact of  
 415 water saturation is negligible, which is also noticed in Table 6. However, from the threshold  
 416 air velocity of 1.0  $m/s$ , which is necessary to reach a fully developed turbulent flow, these  
 417 differences increase significantly. The exchanged energy is at its highest at the saturated  
 418 condition. Conversely, it is at its least at the dry condition. Furthermore, these differences  
 419 become greater as air velocity increases. At an air velocity of 4.0  $m/s$ , the relative difference  
 420 between dry and saturated conditions reach 46.4 % for heating and 42.4 % for cooling.

421

## 422 5. Conclusion

423 In summary, based on the recorded data of the instrumented EAHE site over a long period,  
 424 the impact of soil moisture content on the long-term energy performance of the entire EAHE  
 425 system was studied in this work.

426 Soil thermal properties at different water moistures were measured by using the heat-pulse  
 427 dual probe and the stationary guarded hot plate device according to their textures. Based  
 428 on these measurements, an analytical approach was proposed to determine the evolution of  
 429 soil thermal conductivity and heat capacity depending on sand content, dry density and soil  
 430 water saturation. The proposed approach was used to estimate the thermal properties of 3  
 431 soil layers of the EAHE site.

432 To assess the long-term energy performance of the EAHE system, a numerical simulation

433 framework was proposed. By using external ambient air temperature, the evolution of soil  
434 temperature at the depth of exchanger pipe was estimated. The output air temperature of  
435 the EAHE exchanger was calculated by selecting the suitable impacted soil thickness around  
436 the pipe and the by-pass procedure applied to the system. The proposed model was validated  
437 due to its good performance concerning the simulation of the output air temperature and  
438 the estimation of the cumulated heating and cooling energy for a period of 3 years.  
439 The impact of soil moisture on the long-term energy performance of the EAHE system was  
440 analyzed at dry, partially and fully saturated conditions, by using the proposed analytical  
441 approach of soil thermal properties. A very small impact of soil moisture content is noticed  
442 on the low air circulation velocity but a significant difference is noticed when air velocity was  
443 greater than the threshold value to reach the fully developed turbulent flow. This difference  
444 reaches more than 40 % for the maximum recommended air velocity of 4.0 *m/s*.

## 445 Acknowledgements

446 This work is funded by the the European Commission Initiative INTERREG IV, Upper  
447 Rhine Programme (Project B20-TEM3). The authors thank Jean-David GRANDGEORGE  
448 and Daniel EICH for their assistance in the conception and installation of the EAHE exper-  
449 imental site.

## 450 References

- 451 [1] Florides, G., Kalogirou, S.. Ground heat exchangers-a review of systems, models and  
452 applications. *Renewable Energy* 2007;32(15):2461–2478.
- 453 [2] Thiers, S., Peuportier, B.. Thermal and environmental assessment of a passive building  
454 equipped with an earth-to-air heat exchanger in france. *Solar Energy* 2008;82(9):820–  
455 831.
- 456 [3] Bisoniya, T.S., Kumar, A., Baredar, P.. Experimental and analytical studies of  
457 earth–air heat exchanger (eahe) systems in india: A review. *Renewable and Sustainable*  
458 *Energy Reviews* 2013;19(0):238 – 246.
- 459 [4] Seneviratne, S.I., Corti, T., Davin, E.L., Hirschi, M., Jaeger, E.B., Lehner, I.,  
460 et al. Investigating soil moisture-climate interactions in a changing climate: A review.  
461 *Earth-Science Reviews* 2010;99(3-4):125 – 161.
- 462 [5] Vereecken, H., Huisman, J., Pachepsky, Y., Montzka, C., van der Kruk, J., Bogaen,  
463 H., et al. On the spatio-temporal dynamics of soil moisture at the field scale. *Journal*  
464 *of Hydrology* 2014;516:76 – 96.
- 465 [6] Manstretta, V., Rossi, V.. Modelling the effect of weather on moisture fluctuations in  
466 maize stalk residues, an important inoculum source for plant diseases. *Agricultural and*  
467 *Forest Meteorology* 2015;207:83 – 93.
- 468 [7] Woodside, W., Messmer, J.. Thermal conductivity of porous media. i. unconsolidated  
469 sands. *Journal of Applied Physics* 1961;32(9):1688–1699.

- 470 [8] Tavman, I.. Effective thermal conductivity of granular porous materials. *International*  
471 *Communications in Heat and Mass Transfer* 1996;23(2):169–176.
- 472 [9] Abu-Hamdeh, N.H.. Thermal properties of soils as affected by density and water content.  
473 *Biosystems Engineering* 2003;86(1):97 – 102. Soil thermal properties under pressure.
- 474 [10] Usowicz, B., Lipiec, J., Ferrero, A.. Prediction of soil thermal conductivity based on  
475 penetration resistance and water content or air-filled porosity. *International Journal of*  
476 *Heat and Mass Transfer* 2006;49(25-26):5010 – 5017.
- 477 [11] Lipiec, J., Usowicz, B., Ferrero, A.. Impact of soil compaction and wetness on thermal  
478 properties of sloping vineyard soil. *International Journal of Heat and Mass Transfer*  
479 2007;50:3837 – 3847. Soil thermal properties under pressure.
- 480 [12] Davarzani, H.b., Marcoux, M.b., Quintard, M.b.. Effect of solid thermal conductivity  
481 and particle-particle contact on effective thermodiffusion coefficient in porous media.  
482 *International Journal of Thermal Sciences* 2011;50(12):2328–2339.
- 483 [13] Gori, F., Corasaniti, S.. New model to evaluate the effective thermal conductivity of  
484 three-phase soils. *International Communications in Heat and Mass Transfer* 2013;47(0):1  
485 – 6.
- 486 [14] Nikiforova, T., Savytskyi, M., Limam, K., Bosschaerts, W., Belarbi, R.. Methods  
487 and results of experimental researches of thermal conductivity of soils. *Energy Procedia*  
488 2013;42(0):775 – 783. *Mediterranean Green Energy Forum 2013: Proceedings of an*  
489 *International Conference MGEF-13*.
- 490 [15] Nowamooz, H., Nikoosokhan, S., Lin, J., Chazallon, C.. Finite difference model-  
491 ing of heat distribution in multilayer soils with time-spatial hydrothermal properties.  
492 *Renewable Energy* 2015;76:7 – 15.
- 493 [16] Leong, W., Tarnawski, V., Aittomäki, A.. Effect of soil type and moisture content  
494 on ground heat pump performance: Effet du type et de l’humidité du sol sur la perfor-  
495 mance des pompes à chaleur à capteurs enterrés. *International Journal of Refrigeration*  
496 1998;21(8):595 – 606.
- 497 [17] Mohamed, M., Kezza, O.E., Abdel-Aal, M., Schellart, A., Tait, S.. Effects of coolant  
498 flow rate, groundwater table fluctuations and infiltration of rainwater on the efficiency  
499 of heat recovery from near surface soil layers. *Geothermics* 2015;53(0):171 – 182.
- 500 [18] Gao, Y., Fan, R., Li, H., Liu, R., Lin, X., Guo, H., et al. Thermal performance im-  
501 provement of a horizontal ground-coupled heat exchanger by rainwater harvest. *Energy*  
502 *and Buildings* 2016;110:302 – 313.
- 503 [19] Platts, A.B., Cameron, D.A., Ward, J.. Improving the performance of ground coupled  
504 heat exchangers in unsaturated soils. *Energy and Buildings* 2015;104:323 – 335.
- 505 [20] Sipio, E.D., Bertermann, D.. Soil thermal behavior in different moisture condition: an  
506 overview of iter project from laboratory to field test monitoring. *Environmental Earth*  
507 *Sciences* 2018;(77).

- 508 [21] Vaz, J.b., Sattler, M., Dos Santos, E., Isoldi, L.. Experimental and numerical analysis  
509 of an earth-air heat exchanger. *Energy and Buildings* 2011;43(9):2476–2482.
- 510 [22] Gan, G.. Dynamic interactions between the ground heat exchanger and environments  
511 in earth–air tunnel ventilation of buildings. *Energy and Buildings* 2014;85(0):12 – 22.
- 512 [23] Gan, G.. Simulation of dynamic interactions of the earth–air heat exchanger with soil  
513 and atmosphere for preheating of ventilation air. *Applied Energy* 2015;158:118 – 132.
- 514 [24] Gan, G.. Dynamic thermal simulation of horizontal ground heat exchangers for renew-  
515 able heating and ventilation of buildings. *Renewable Energy* 2017;103:361 – 371.
- 516 [25] Cuny, M., Lin, J., Siroux, M., Magnenet, V., Fond, C.. Influence of coating soil  
517 types on the energy of earth-air heat exchanger. *Energy and Buildings* 2018;158:1000 –  
518 1012.
- 519 [26] KD2Pro, . KD2 Pro thermal properties analyzer - Operator’s Manual. Decagon Devices  
520 Inc.; 2011.
- 521 [27] Carslaw, A.. *Conduction of heat in solid*. 2nd ed. London: Oxford; 1959.
- 522 [28] Kluitenberg, G.J., Ham, J.M., Bristow, K.L.. Error analysis of the heat pulse method  
523 for measuring soil volumetric heat capacity. *Soil Science Society of America Journal*  
524 1993;57(6):1444–1451.
- 525 [29] ISO 8302:1991(E). Thermal insulation – determination of steady-state thermal resis-  
526 tance and related properties – guarded hot plate apparatus. Standard; International  
527 Organization for Standardization; 1991.
- 528 [30] Kersten, M.S.. *Thermal Properties of Soils*. University of Minnesota; 1949.
- 529 [31] Cote, J., Konrad, J.M.. A generalized thermal conductivity model for soils and con-  
530 struction materials. *Canadian Geotechnical Journal* 2005;42(2):443–458.
- 531 [32] Cuny, M., LIN, J., Siroux, M., Fond, C.. Simplification of boundary condi-  
532 tions of the modeling of shallow geothermalsystems. *French Thermal Congress 2015,La*  
533 *Rochelle,France 2015;*
- 534 [33] Hollmuller, P.. Analytical characterisation of amplitude-dampening and phase-  
535 shifting in air/soil heat-exchangers. *International Journal of Heat and Mass Transfer*  
536 2003;46(22):4303–4317.
- 537 [34] SACADURA, J.F.. *Transferts thermiques-Initiation et approfondissement*. Lavoisier;  
538 2015.
- 539 [35] HERNOT, D., PORCHER, G.. *Thermique appliquee aux batiments*. CFP; 1984.
- 540 [36] VDI4604: Part4. Thermal use of the underground-direct uses. Standard; Verein  
541 Deutscher Ingenieure VDI-GET; 2004.